Indian Journal of Geo Marine Sciences
Vol. 51 (11), November 2022, pp. 918-929
DOI: 10.56042/ijms.v51i11.3509

Application of liberation analysis in ferromanganese encrustations from South Andaman Sea: An automated mineral identification technique using TIMA

R V Manoj*[,a], P R Rajani[b], M Girish Kumar[c], B Gopakumar[d], R K Joshi[e] & S Resmi[f]

[a]Geological Survey of India, Pandeshwar, Mangalore, Karnataka – 575 001, India
[b]Geological Survey of India, Seminary Hills, Nagpur, Maharashtra – 440 006, India
[c]Geological Survey of India, CHQ, Kyd Street, Kolkata, West Bengal – 700 091, India
[d]Geological Survey of India, Jhalana Doongri, Jaipur, Rajasthan – 302 004, India
[e]Geological Survey of India, Bhopalpani, Dehradun, Uttarakhand – 248 008, India
[f]Geological Survey of India, Aliganj, Lucknow, Uttar Pradesh – 226 024, India
*[E-mail: manoj.rv@gsi.gov.in]

Received 07 June 2021; revised 22 November 2022

Automated scanning electron microscopic studies got wide acceptance in identification of various mineral phases; its classification and characterization based on their composition and abundance in semi quantitative manner. Nowadays, these techniques are adopted in understanding various poorly crystalline and amorphous materials to reveal the actual mineral assemblages. Primary mineral phases of five ferromanganese crust and nodule samples collected from West Sewell Ridge and Sewell Rise in South Andaman Sea are studied using automated mineral analyser to understand the mineral assemblages and their micro textures. The internal morphology of these encrustations is densely parallel to sub parallel micro botryoidal textures indicating colloidal precipitated origin from ambient seawater. Since crust and nodules are formed by colloidal precipitation, unclassified materials observed in primary phase analyses may represent the presence of poorly crystalline and amorphous ferromanganese colloidal phases. The liberation analysis, Back Scattered Electron image (BSE), Energy Dispersive X-ray Spectroscopy (EDS), and elemental mapping of the samples revealed occurrence of manganese - iron oxy-hydroxides as alternate laminations/ thin layers along with detrital materials; that forms the composition and internal texture. Major mineral phases identified from liberation analysis using TIMA are todorokite, vernadite, Fe vernadite, cryptomelane, ferrogedrite, glauconite, Fe oxides disseminated, quartz, biotite, orthoclase, illite, plagioclase, amphibole, zinwaldite, and romanechite. Thus, automated mineral identification using TIMA can be effectively adopted for mineral phase identification in ferromanganese encrustations, which is rather difficult using other techniques.

[**Keywords**: Ferromanganese encrustations, Liberation analysis, Primary phase, Scanning electron microscope, Sewell Rise, TIMA, West Sewell Ridge]

Introduction

In earth science, technologies like optical microscopy, X-ray Diffraction (XRD)[1], Scanning Electron Microscope (SEM), and Electron Probe Microanalysis (EPMA) are widely utilized to identify rocks, determination of mineral phase chemistry, elemental mapping, and semi quantitative analysis along with detailed petrographic studies. Although XRD is the appropriate method for identification of crystalline phases[1], determination of amorphous and cryptocrystalline phases formed by authigenic precipitation and other low temperature processes is intricate using XRD. In EPMA and SEM analyses, information regarding texture and chemical composition of the samples are extracted by Secondary Electron (SE) and Backscattered Electron (BSE) imaging[2-4]. BSE imaging along with Energy Dispersive X-ray Spectroscopy (EDS) in SEM is capable of determination of semi-quantitative chemical composition of the samples. Wavelength Dispersive Spectroscopy (WDX) in EPMA is an enhanced technique for quantitative measurement of the chemical composition. However, both these techniques require manual modal calculations using the chemical components to determine the mineral phases. In recent years, automated scanning electron microscopy have been used for various scientific studies in rapid quantification and characterization of minerals[3-10]. It is a combined technique of backscatter imaging along with four EDS detectors for highly sensitive spectral summing, which helps in generating mineralogical data by identification and quantification

of mineral phases automatically using algorithms set in based on built-in mineralogical database[6].

TESCAN Integrated Mineral Analyser (TIMA) is primarily used for automated mineral modal analysis directed for quantitative mineral mapping[8,9]. The mineral distribution data are obtained by matching the acquired spectral data with TESCAN mineral database. This method of BSE and EDS combined high-resolution mineral mapping using SEM were initially employed for mineral processing and ore characterisation[8]. TIMA can produce mineralogical data based on their elemental abundance in more advanced way over the normal scanning electron microscopic technique. Combined high resolution primary phase mineral mapping along with backscatter imaging and energy dispersive spectrum are used to determine mineral assemblages in wide range, their distribution, textures, grain size, quantification and its association with the help of bright phase analysis.

Many workers used various basic to advanced techniques to understand the physical properties, texture, morphology, mineralogy, petrogenesis, composition and disposition of laminations[11-20]. Recently, some studies reported extensive occurrence of ferromanganese crust and nodules from South Andaman Sea and studied the morphology of the ferromanganese encrustations[21-25]. Bulk chemical analyses of the samples from South Andaman Sea showed relatively high enrichment of Rare Earth Elements (REE), Platinum Group Elements (PGE), and other trace elements, which are of economic importance[24,25]. To identify various assemblages of minerals in the studied sections advanced techniques like automated mineral mapping were adopted to extract maximum information on mineral assemblages. The preliminary petrographic studies of ferromanganese nodules and crust was carried out to identify texture, type of laminations, layer disposition, and hiatus in precipitation of the ferromanganese oxy hydroxides under reflected light (Fig. 1).

The present study focuses on the application of liberation analyses using TIMA for the identification of major and minor mineral assemblages in the ferromanganese crust and nodule samples from South Andaman Sea. The study attempts to understand the mineralogical assemblages by using high resolution automated mineral mapping of the Fe Mn laminations

Fig 1 — Photographs of hand specimen of ferromanganese nodules and crust collected from West Sewell Ridge and Sewell Rise in South Andaman Sea showing surface textures and properties such as sugary, botryoidal with current polished surfaces

in the crust and nodules collected from southern part of West Sewell Ridge as well as from the southern part of the Sewell Rise in South Andaman Sea. Along with aforementioned primary objective, present work is an attempt to bring out the microstructures, textures, forms of crust and nodules and their genetic significance prevailed during the precipitation of colloids.

Materials and Methods

Ferromanganese encrustations and nodules occur as pavements over sediments and hard substrates in various topographic highs in the South Andaman Sea[21]. Remotely Operated Vehicle (ROV) and Grab sampler was deployed to obtain samples at depth ranges between 550 m and 1450 m water depth. The collected samples were dark brown to pitch black in colour and show botryoidal to sugary texture with rough to irregular surface. Surface of the encrustations are often smoothened due to bottom current activity present in the area. Prominent growth layers of ferromanganese oxy-hydroxides of thickness varying from 0.5 to 5 cm are observed in the sections. The laminations are normally parallel, columnar and show micro botryoidal pattern. The alternative laminations are mainly ferromanganese oxides representing the greyish brown to metal black colour along with intercalations of detrital quartz grains and bioclasts[26], especially foraminifera.

For TIMA, thin sections are made on an automated thin-section preparation machine by following standard procedures to prepare ~30-micron thick sections, bound by epoxy resin base on glass slide having dimension ~46 mm × 30 mm × 1.2 mm and polished. Thin sections of the ferromanganese crust and nodules were studied under microscope for preliminary understanding of the micro textures.

The TESCON Integrated Mineral Analyser (TIMA) technique is applied for selected thin section of ferromanganese crust and nodules. TIMA is used for automated mineralogy system for fast quantitative analysis with combinations of BSE and EDX analyses to identify minerals, its concentrations, element distributions, and mineral texture properties[9,10]. TIMA uses EDAX element silicon drift detectors that increases sensitivity to light elements and maintain stable energy resolution at very high counts. The TIMA software used for the analyses includes new mineral generation tools and low element detection limit using patented pixel analysis algorithms. Instrument consists of complete hardware integration of X-ray acquisition and beam scanning system with mineral classification schemes.

In area of interest, BSE analysis along with EDS spectrum are acquired to define the grain boundaries and compositional variations. Mineral classification using TIMA can identify minerals by assigning composition using EDS analysis. Analyses are done with accelerating voltage of 15 – 20 kV and an electron beam current of 12 nA focused to 1 μm spot size as operating conditions[4]. The liberation analysis module covers the analytical location in polished section by equally distant parallel horizontal lines using a stated line space. The samples are analysed under the BSE, primary phase, spectrum, elemental mapping and line/point analysis mode; and quantitative energy-dispersive X-ray spectroscopic analysis are performed with an EDS system attached to SEM for obtaining the composition and mineral assemblage.

Results

Under reflected light in petrographic microscope, isotropic laminations with medium to high reflectivity were observed. The internal layers normally vary from dense parallel to sub parallel laminations, botryoidal, globular, mixed and stromatolitic in nature. The high reflective layers represent the manganese rich layers that are thick to thin continuous in nature and some are also discontinuous. Abundant bioclasts such as foraminiferal tests were identified in samples, where the bioclasts are embedded and later mineralized due to enrichment of Mn during deposition[15,26]. Poly nucleated concentric growth laminae are observed in the sections. TIMA observations reveals that the manganese - iron oxy-hydroxides occurs as parallel layers and laminations, cemented with silica and other detrital materials, that together forms the micro structure and textures representing minerals and internal morphology of ferromanganese crust and nodules.

Ferromanganese nodules

From liberation analysis using TIMA – primary phase model results of ferromanganese nodule (ROV R2/2 – Fig. 2a & b) has revealed the presence of todorokite (Mn rich phase), vernadite, Fe-vernadite as dominant phases along with minor phases of quartz, illite, plagioclase, amphiboles, cryptomelane and disseminated Fe-oxides (Table 1). The detritus minerals dominated by quartz and plagioclase feldspar occur as intercalations with Mn and Fe phases. The unclassified mineral phases present in the

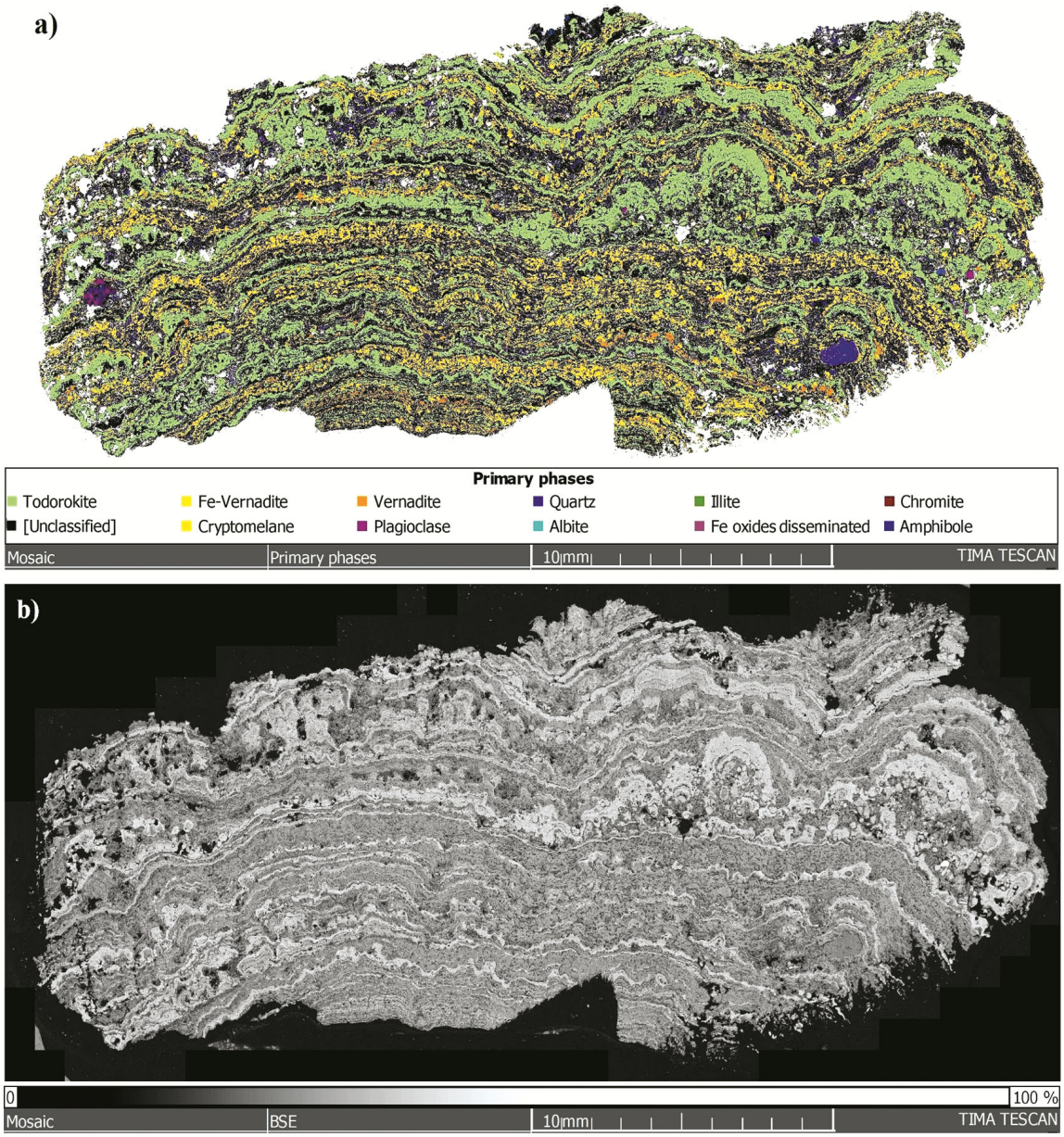

Fig 2 — TIMA liberation analysis images of R2/2 Ferromanganese nodule: (a) Primary phase analysis image reflecting integrated mineral mapping of the thin section with MnO rich (Todorokite) layers disposed in micro botryoidal texture and FeO rich laminations along with detrital minerals; and (b) BSE image of the section showing compositional variation. Lighter layers depict Mn-rich and darker layers indicate Fe rich phases

analyses may be representing the amorphous phases of Mn and Fe oxy-hydroxide phases accumulated during colloidal precipitation.

Elemental mapping also shows the Mn rich phase-todorokite (Fig. 3a), Fe rich - Vernadite and Vernadite (Fig. 3b) enriched layers as alternate bright phase laminations; while, Si rich (Fig. 3c) and Cobalt enriched domains (Fig. 3d) shows inference to Fe rich layers. The internal structure of the nodule is identified as densely laminated, parallel to sub parallel, micro botryoidal type. The alternative Mn-Fe oxy-hydroxides are indicated by alternate bright and dark laminations. The Mn oxides are abundant towards the outer rim, which represents thick layers. The quantitative weight percentage of the sample reveals unclassified (41.55 %), todorokite (32.41 %), Fe-vernadite (17.1 %), vernadite (3.34 %), quartz (2.74 %), illite (0.55 %), Fe oxides (0.22 %), and

Table 1 — Various mineral phases identified on five ferromanganese crust and nodules samples in South Andaman Sea using TESCON Integrated Mineral Analyzer (TIMA) technique

R2/2	6/4	10/3	R11/2	18
Todorokite	Todorokite	Vernadite	Todorokite	Fe Vernadite
Vernadite	Vernadite	Fe Vernadite	Quartz	Quartz
Fe Vernadite	Fe Vernadite	Cryptomelane	Glauconite	FeO disseminated
Quartz	Cryptomelane	Todorokite	Vernadite	Todorokite
Illite	Ferrogedrite	Quartz	Fe Vernadite	Ferrogedrite
Plagioclase	Glauconite	Fe Oxides	Illite	Albite
Amphiboles	Quartz	Ferrogedrite	Ferrogedrite	Vernadite
Cryptomelane	Biotite	Zinwaldite	FeO disseminated	Plagioclase
FeO disseminated	Orthoclase	Biotite	Romanechite	Illite
	Illite	Orthoclase	Amphibole	Orthoclase
	Plagioclase	Illite	Plagioclase	
	Amphibole	Plagioclase	Albite	
		Amphibole	Biotite	
			Zinwaldite	
			Orthoclase	
			Cryptomelane	

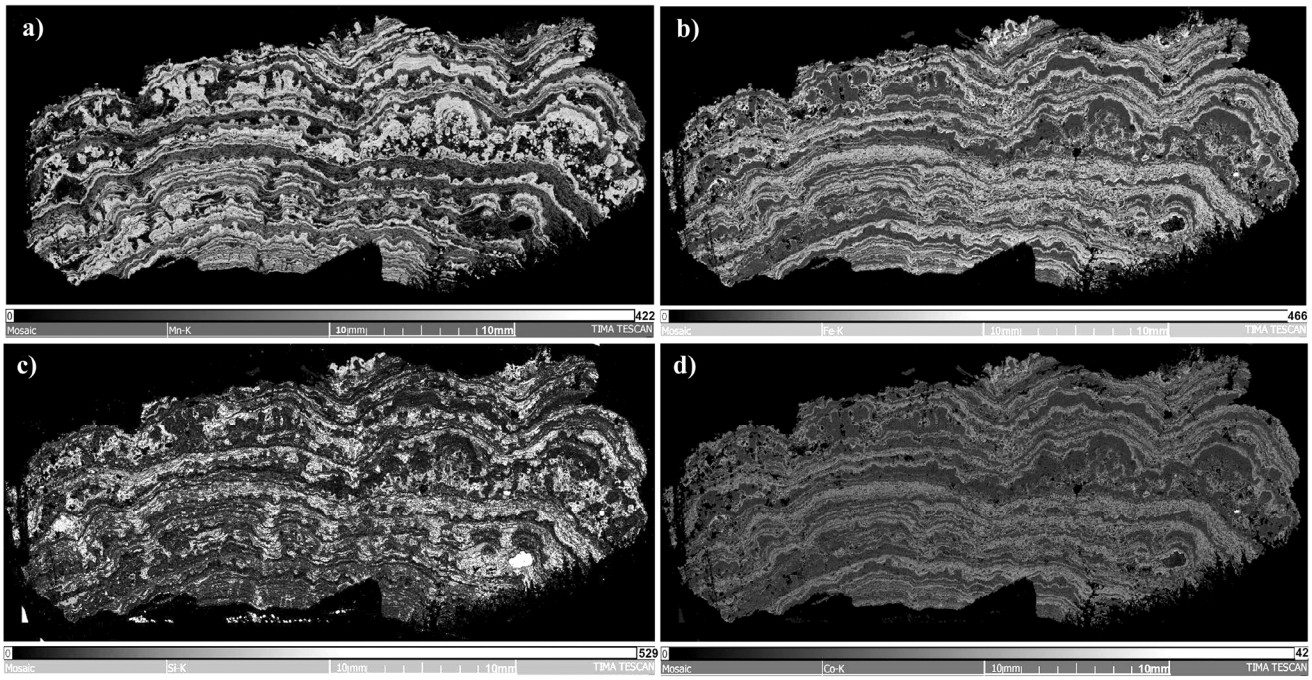

Fig 3 — TIMA elemental analysis of ROV-R2/2 Ferromanganese nodule: (a) Mn elemental mapping showing thick Mn rich layers (Todorokite & Vernadite); (b) Fe elemental mapping image showing Fe oxide (Fe Vernadite) enrichment; (c) Si elemental map showing bright phase images of Si rich domains; and (d) Cobalt elemental maps with Co enriched layers, which have correlation to Fe rich laminations

plagioclase (0.19 %), respectively. From *Webmineral* database preloaded with TIMA software is used for the identification of majority of the mineral phases. Elemental scan for six (Mn-Fe-Si-Co-Ni) elements were shown in various RGB colour combinations with Co and Ni having poor response; while, Si forming prominent detrital (Fig. 4). Line scan was carried out from inner to outer rim of the same sample, which shows Mn-Fe-Si elements are inversely proportional to each other and Mn enrichment is high in centre to inner laminations compared to outer area (Fig. 5).

The Sample ROV-6/4 (Fig. 6a & b) shows major and minor mineral assemblages: todorokite (Mn rich phase), vernadite, Fe vernadite, cryptomelane as dominant phases with minor presence of ferrogedrite, glauconite, quartz, biotite, orthoclase, illite,

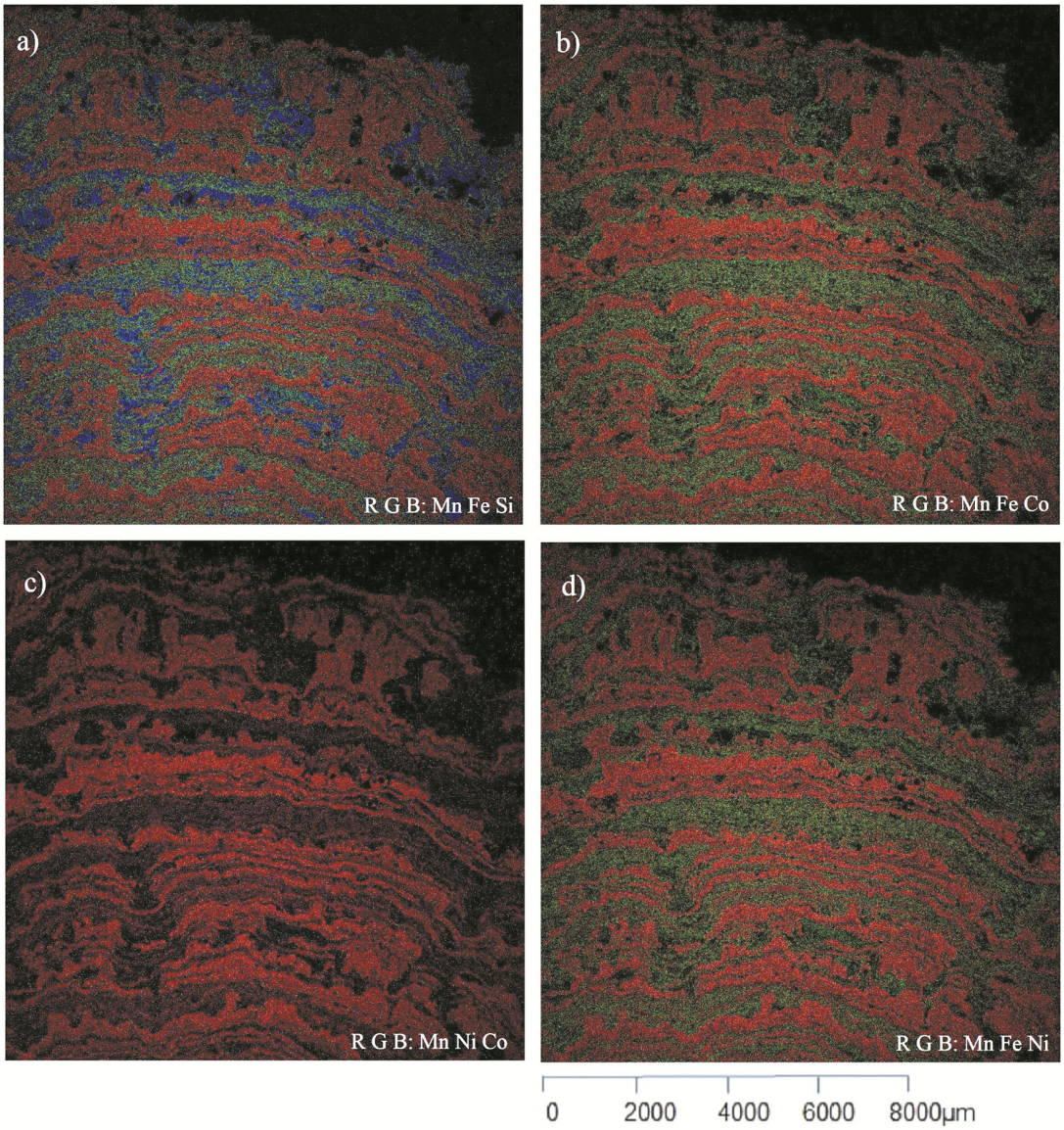

Fig 4 — SEM quantitative elemental maps of major elements in ROV-R2/2: (a) Mn Fe Si disposition shown in RGB colour variations where Mn are dominant throughout the AOI; (b) RGB Mn-Fe-Co; (c) RGB Mn-Ni Co; and (d) RGB Mn-Fe-Ni, where Co & Ni have very minimal response compared to major phases

plagioclase and amphiboles, etc. The studied sections of 40 µm length reflects thick Mn rich layers exhibiting micro botryoidal texture. Mn rich layer varies from 44 to 48 % and oxides are in the range of 41 to 44 % with minor quantities of Mg, Na, Ca, Al, K and Si, that may represent todorokite. Another major phase represents 31 % Fe, 15 % Mn and 42 % oxide followed by minor Ca, Mg, Al, P and Si, which represent Fe vernadite. SEM elemental mapping images shows the Fe oxide and Mn rich todorokite phase (Fig. 6c & d) where the former is enriched compared to latter phase.

In section ROV-10/3 (Fig. 7) liberation analysis shows the BSE and primary phase data with mineral assemblages of vernadite, Fe vernadite, cryptomelane, todorokite and quartz as major phases along with minor phase of Fe oxides, ferrogedrite, zinwaldite, biotite, orthoclase, illite, plagioclase and amphiboles, etc. In this sample FeO forms the dominant unit followed by alternative Mn oxide as thin fine laminations towards the core of the nodule and vice versa. Liberation mapping images of Fe-Mn nodule R-11/2 (Fig. 8) reveals MnO rich todorokite layers disposed in micro botryoidal laminations towards the

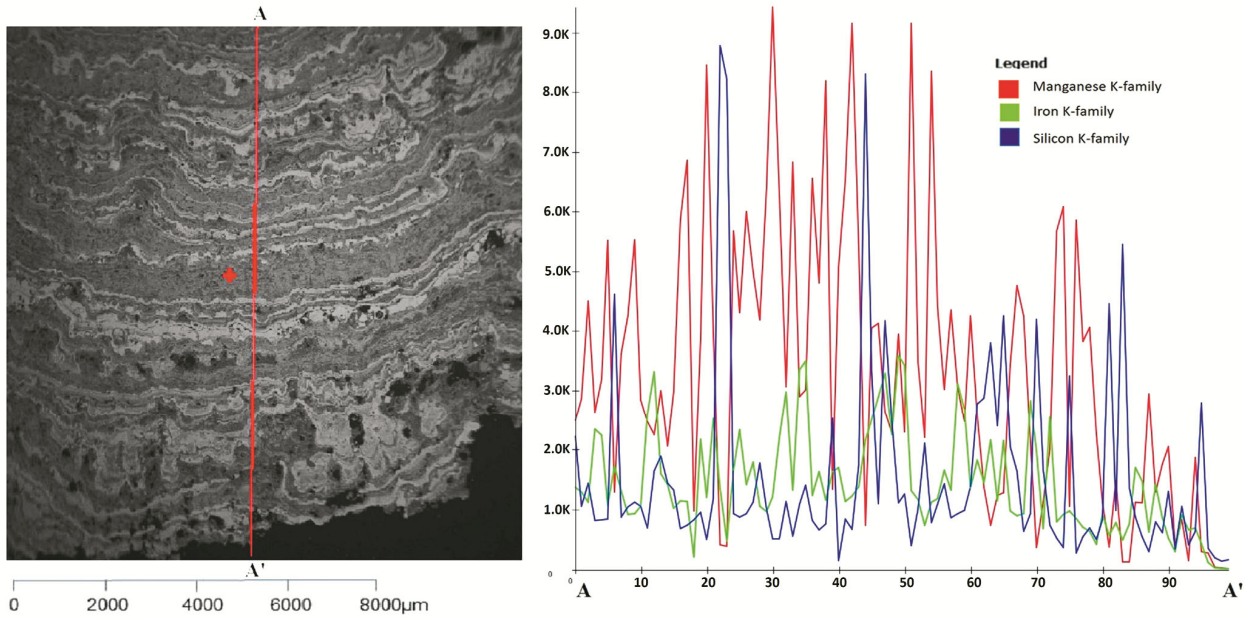

Fig 5 — SEM line scanning image from sample R2/2 inner to outer, Fe Mn laminations shows abundance of the Fe enrichment toward inner part while Mn abundance is high in centre

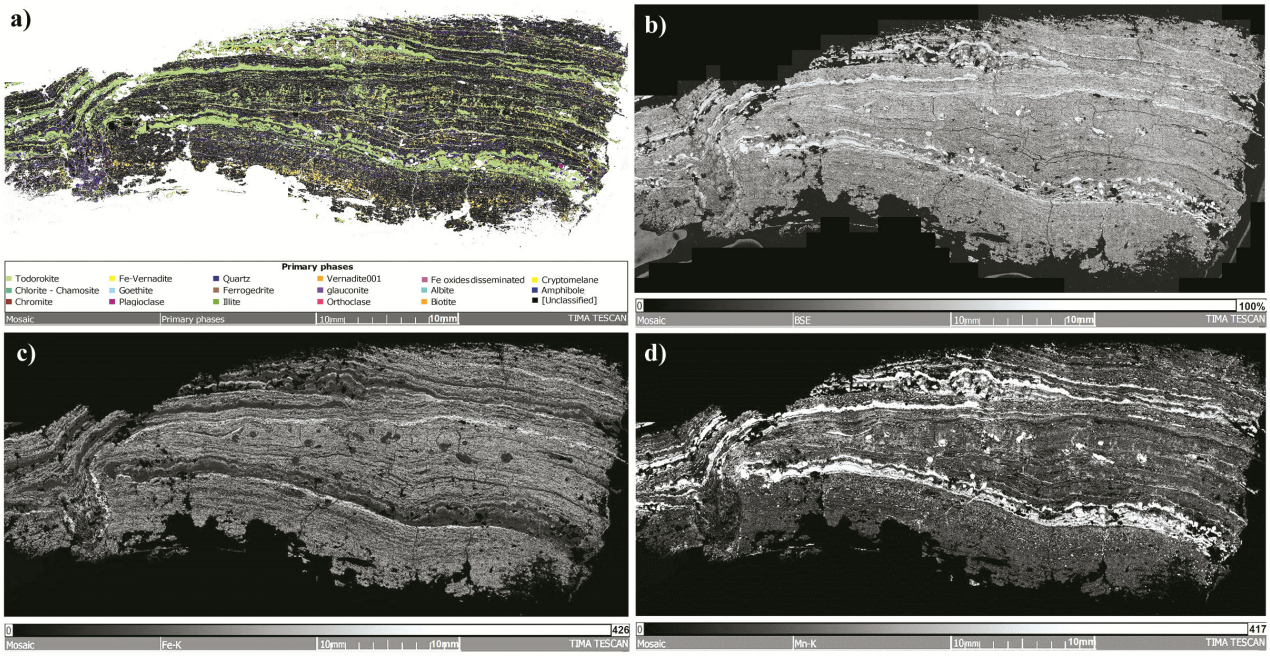

Fig 6 — TIMA liberation mapping images of ROV-6/4: (a) primary phase analysis image reflects the integrated mineral mapping showing MnO rich Todorokite layers disposed in micro botryoidal laminations which are dense throughout in outer and inner layers compared to centre; (b) BSE image with alternate laminations as bright grey of Mn to dark grey Fe layers; (c) Fe oxide rich (Fe Vernadite & Vernadite) thin laminations; and (d) elemental mapping showing Mn rich layers probably of Todorokite

core region, which are dense, while Si rich detrital represents the non-precipitation period. Glauconite layers in between the Mn and Fe laminations indicate the iron rich hydrous silicate, which might have formed substituting the Fe Oxides.

Ferromanganese crust

SEM images of Fe-Mn crust shows the globular-subrounded to rounded growth of micro-nodule with high Fe content. TIMA – Liberation analysis on ROV-18 sample (Fig. 9) reflects the mineral assemblages

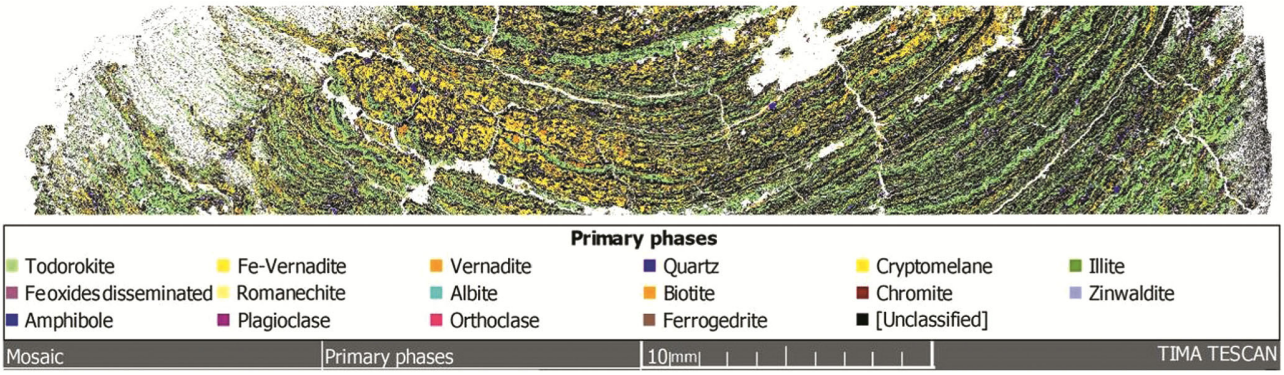

Fig 7 — TIMA liberation mapping images of ROV-10/3 section: Primary phase liberation analysis shows Fe enrichment with dense thin laminations of Vernadite, Fe Vernadite, Cryptomelane, Todorokite and Quartz as major phases

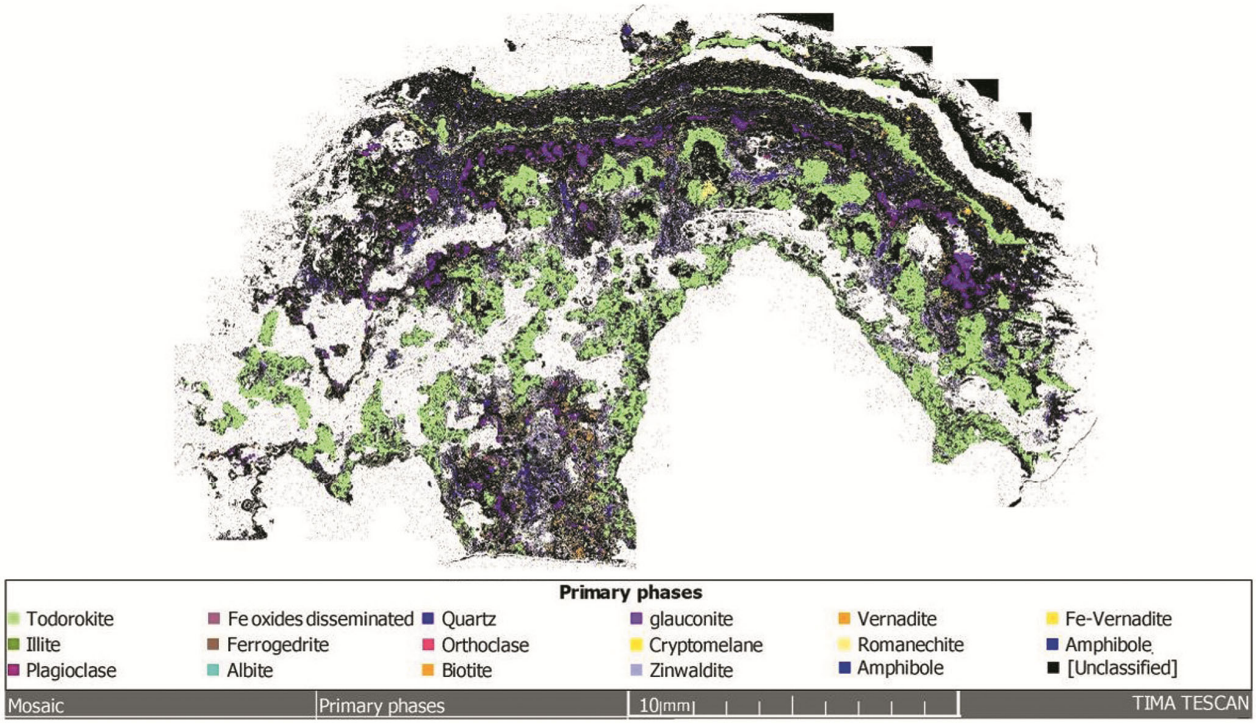

Fig 8 — TIMA liberation mapping images of R-11/2: Glauconite layers in between the Mn and Fe laminations indicate the iron rich hydrous silicate, which might have formed substituting the Fe oxides

such as Fe-vernadite quartz, Fe oxides, todorokite (Mn rich phase), ferrogedrite, albite, vernadite, amphibole, plagioclase, illite and orthoclase, etc. The crust samples are mainly dominated by FeO rich laminations with associated MnO. From the liberation analysis, the Si phase is dominant along with FeO content indicating a continuous non-precipitation period. Bright phase analysis of ROV-18 shows regions of enriched phases of Mn, Fe and Si, where Fe and Si are dominant in crust compared to nodules. The manganese oxide phase especially todorokite and vernadite are intermixed, which are either amorphous or low crystalline in nature. Energy dispersive spectrum of ferromanganese sample ROV-6/4 (Fig. 10a – c) shows the manganese rich spectrum in semi quantitative manner using EDS spectral analysis.

Discussion

The morphology of the ferromanganese crust and nodules depends on the source and influx of the colloidal solution, mineralogy, crystallinity, depositional environment, sedimentation rate, hydrothermal inputs, bottom water currents, substrata, form of nucleus, age, growth rate, hiatus, and

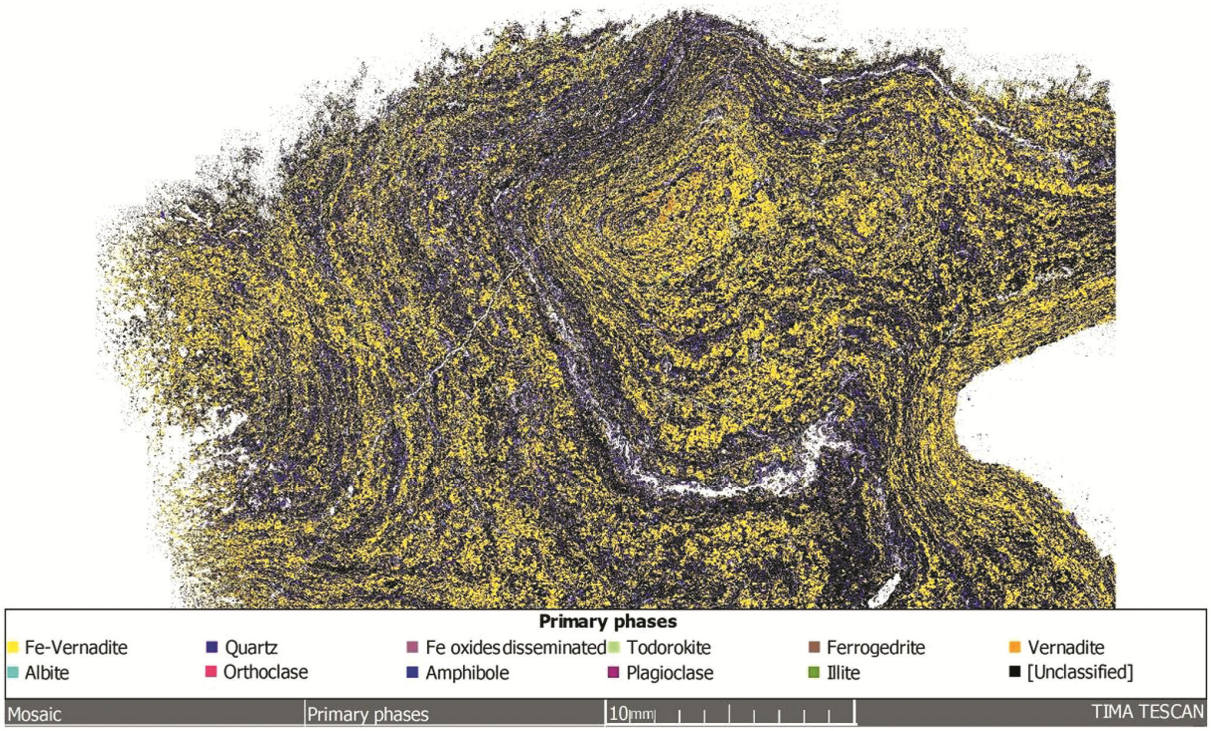

Fig 9 — TIMA liberation mapping images of ROV-18 section showing Fe Vernadite as major constituent with quartz as detrital materials

diagenesis. The discontinuous layers or thinning of the particular layers may indicate the low influx of the colloids or even a possible hiatus. The low to intermediate reflectivity indicates Fe rich, Fe-Mn mixed, or admixtures of other major elements. In the saddle areas of the laminations, brecciated quartz and other detritals are noted, which also indicate the non-precipitation or hiatus. These primary microstructures and textures indicate that the nodules formation was episodic. Micro-stromatolitic growth bands and elongated segregates in each band or lamina indicates possible direction of growth. Multinucleated growth laminations indicate the earlier formed nodules which acted as a nucleus for the accretion of ferromanganese oxides.

From detailed scanning electron microscope studies, alternate dark and light grey colour bands represent different depositional environments with variations in their geochemical parameters. The bright layers indicate Mn rich phase todorokite with intermediate Fe laminations, and the growth structure predominantly depends on the colloids influx and depositional environment[6]. The laminations are normally parallel, columnar and shows micro botryoidal pattern indicating hydrogenetic origin. Some of the Mn-Fe phases are amorphous to low crystalline that are difficult to detect under liberation analysis. BSE and primary phase analyses indicate two distinct growth episodes characterized by textural and compositional variations. The growth episodes of nodules indicate dense todorokite phase intermixed with thin laminations of Fe-vernadite, but towards the rim, dominance of todorokite and Mn rich phase with micro-botryoidal texture can be observed. Individual laminations show compositional variations, probably representing the depositional environment prevailed during its formations.

Depositional hiatuses indicate that the growth of the oxide layers is not always continuous but the period of the hiatuses remains unknown. The lighter bands are more enriched in manganese content along with iron, whereas the darker bands have enriched in iron content compared to the lighter one giving its darker shade. The discontinuous precipitation is mainly due to the various reasons mainly by fracture, growth, burrowing, fluidification, or by alteration[6]. The detrital grains are mostly quartz, plagioclase feldspar and clay minerals, which mainly occur as fracture or void fillings sometimes as continuous laminations. The episodic changes of the colloidal precipitation cause the elemental variations in the laminations, which can be related to the bottom water circulation and elemental

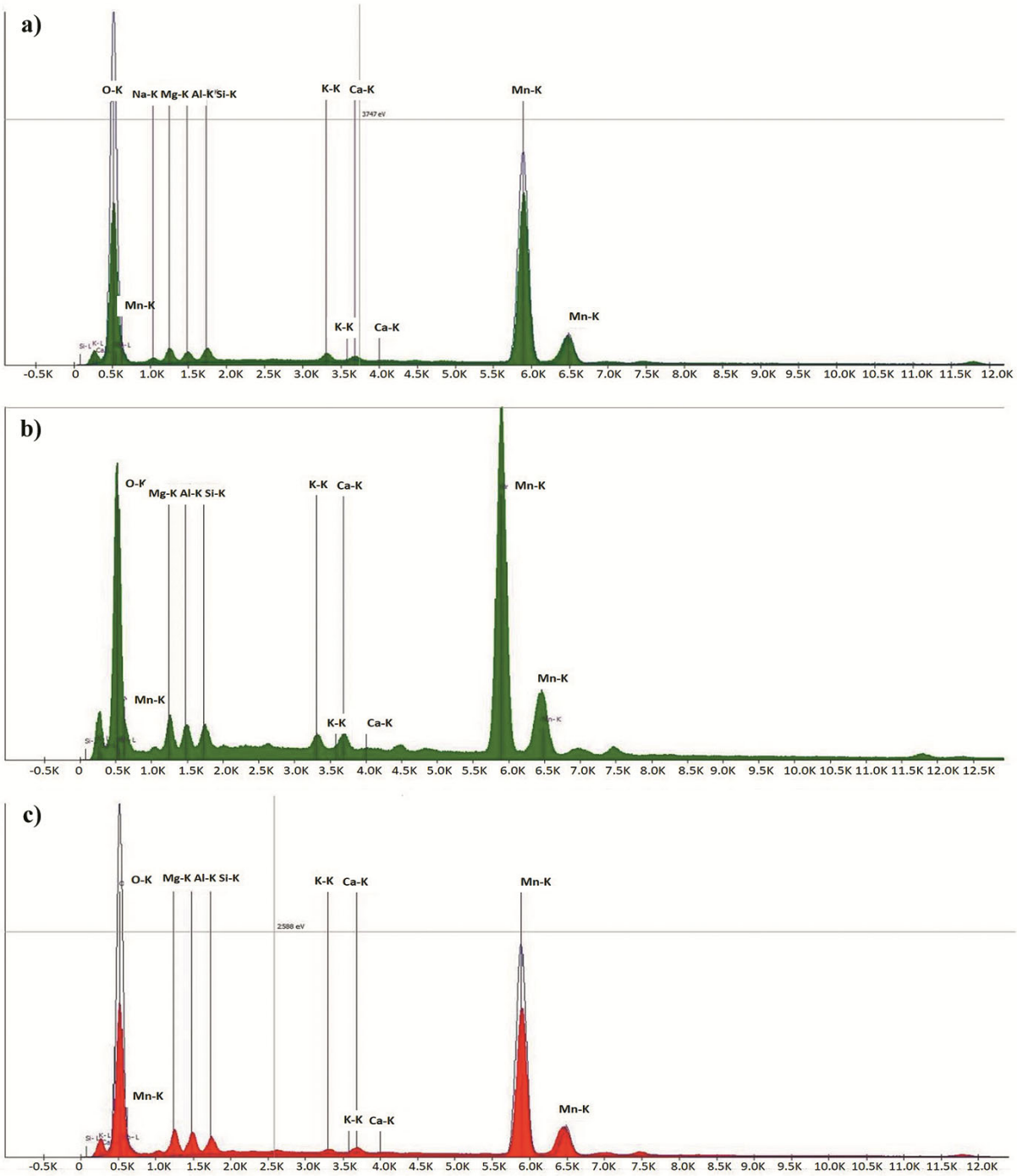

Fig 10 — TIMA EDS spectrum of ferromanganese sample (ROV-6/4): a, b & c shows the manganese rich phases

influx. The presence of good amount of biogenous matter also causes the increase in rate of diagenetic process. Variations in the microstructures of these nodules and crusts can be related to changes in bottom current activity, diagenesis which causes the replacement of the bioclasts to oxide minerals and growth rate under changing oceanographic conditions[26].

From the above observations, it is clear that the ferromanganese crust and nodules from South Andaman Sea have formed as alternate laminations of Fe-Mn rich layers (todorokite, vernadite, Fe vernadite) in a mixed environment of hydrogenetic as well as hydrothermal which is indicated by the presence of other trace elements from geochemical

data[25]. Whereas, various mineral phases and internal morphologies are interbedded with brecciated quartz and detrital. In ferromanganese crust multi nucleated laminations are also identified indicating various growth series.

Summary

i. The internal morphology of the crust and nodules varies from dense parallel to sub parallel laminations, botryoidal, stromatolitic, multi nucleated to globular in nature.

ii. TIMA liberation analysis along with backscatter and elemental mapping reveals that ferromanganese crust and nodules are composed of Mn and Fe rich mineral, todorokite and Vernadite inter laminated with quartz and other detritus minerals.

iii. The various mineral phases identified include todorokite, vernadite, Fe vernadite, cryptomelane, ferrogedrite, glauconite, quartz, biotite, orthoclase, illite, plagioclase, zinwaldite, romanechite and amphibole. Unclassified phases may represent the poorly crystalline and amorphous ferromanganese colloidal phases.

iv. Identification of mineral phases in the ferromanganese crust and nodules by conventional powder diffraction method is a difficult task because of the under developed crystalline phases formed by the colloidal precipitation of Mn and Fe oxyhydroxides from the ambient seawater. Automated mineral analysis by TIMA provides comprehensive mineral classes through elemental mapping and modal analyses, which makes it an effective methodology for understanding the mineralogy and microstructures of ferromanganese crust and nodules.

Acknowledgements

Authors sincerely thank colleagues the onboard SR-045 cruise in the South Andaman Sea, and especially the Chief Scientist and Supervisory Officer under whose supervision the cruise work was undertaken under field season programme 2018-19 for their immense support and encouragement. Authors extends their thanks to the DG, GSI for encouragement and support. Authors are also grateful to the Deputy Director General & HOD, M&CSD, Geological Survey of India (GSI), Mangalore for technical as well as financial assistance for the proposed study and for permission to publish this work. We also thank the Director in charge, NCEGR, GSI, Bengaluru for providing permission to carry out TIMA analysis as a part of the field season programme. Also, the onboard survey along with sampling and processing for petrographic studies rovided by the Operation East Coast-I, M&CSD, GSI, Kolkata is duly acknowledged.

Conflict of Interest

Authors here by certify that all authors contributed the work for the scientific content and overall preparation of the manuscript. Also, certify that this scientific work is not submitted to publish anywhere or other publications. The authors declare no competing or conflict of interest.

Author Contributions

RVM: Conceptualization and drafting, preparation of figures and tables, sample preparation and laboratory work; PRR: Modification of the draft, sample preparation and laboratory work; MGK: TIMA analyses; BG & SR: Sample preparation and laboratory work; and RKJ: Sample selection, preparation and laboratory work.

Ethical Statement

This material is the authors' original work, which is not been published elsewhere. All authors have been personally and actively involved in substantial work leading to the paper, and take responsibility for its content.

References

1 Lindholm R C, Mineral identification using x-ray diffraction, In: *A practical approach to sedimentology*, (Springer, Dordrecht Netherlands), 1987, pp. 124-153. https://doi.org/10.1007/978-94-011-7683-5_6

2 Reed S J B, *Electron Microprobe Analysis and Scanning Electron Microscopy in Geology*, 2nd edn, (Cambridge University Press), 2005, pp. 189. DOI: https://doi.org/10.1017/CBO9780511610561

3 Jones M P, *Applied mineralogy: a quantitative approach*, 1st edn, (Springer, Dordrecht), 1987, pp. 260. ISBN-13: 978-0860105114

4 King R P, Basic image analysis for mineralogy, In: *ICAM'93 Demonstration Workshop Manual*, 1993, pp. 119-139.

5 Gu Y, Automated Scanning Electron Microscope Based Mineral Liberation Analysis, *J Miner Mater Characterization Eng*, 2 (1) (2003) 33-41.

6 Fandrich R, Ying G, Debra B & Kurt M, Modern SEM-based mineral liberation analysis, *Int J Miner Process*, 84 (2007) 310-320. DOI: 10.1016/j.minpro.2006.07.018

7 Ward I, Merigot K & McInnes B I A, Application of Quantitative Mineralogical Analysis in archaeological micromorphology: a case study from Barrow Is., Western Australia, *J Archaeol Method Theory*, 25 (2018) 45-68.

8 Paul G & Marek D, The Use of the TIMA Automated Mineral Analyzer for the Characterisation of Ore Deposits and Optimization of Process Operations, Conference paper presented at the *MinPet, Mineralogy and Petrology, Proceedings of the Austrian Mineralogical Society* (Leoben, Austria), 161, 2015.

9 Hrstka T, Gottlieb P, Skala R, Breiter K & Motl D, Automated mineralogy and petrology - applications of TESCAN Integrated Mineral Analyzer (TIMA), *J Geosci*, 63 (1) (2018) 47-63. DOI: 10.3190/jgeosci.250

10 Shulz B, Sandmann D, Gilbricht S, SEM-Based automated mineralogy and its application in geo- and material sciences, *Minerals*, 10 (11) (2020) p. 1004. DOI: 10.3390/min10111004

11 Marchig V & Halbach P, Internal structures of manganese nodules related to conditions of sedimentation, *TMPM Tschermaks Petr Mitt*, 30 (1982) 81-110. DOI: 10.1007/BF01082497

12 Uspenskaya T Y, Gorshkov A I & Sivtsov A V, Mineralogy and Internal structure of fe-Mn nodules from the Clarion-Clipperton Fracture Zone, *Int Geol Rev*, 29 (3) (1987) 363-371.

13 Banerjee R, Roy S, Dasgupta S, Mukhopadhyay S & Miura H, Petrogenesis of ferromanganese nodules from east of the Chagos Archipelago, Central Indian Basin, Indian Ocean, *Mar Geol*, 157 (1999) 145–158.

14 Hein J R, Cobalt-rich ferromanganese crusts: Global distribution, composition, origin and research activities, In: *Polymetallic massive sulphides and cobalt-rich ferromanganese crusts: Status and prospects*, Proceedings of a workshop help on 26-30 June, 2000, International Seabed Authority, (Kingston, Jamaica), ISA Technical Study, 1 (2004) 188-256.

15 Kumar G & Tiwary S K, Morphology and Geochemistry of the Polymetallic nodules from the Central Indian Ocean Basin, *Int J Chem Sci*, 6 (4) (2008) 2264-2277.

16 Gonzalez F J, Somoza L, Lunar R, Martinez-Frias J, Martin Rubí J A, *et al*., Internal features, mineralogy and geochemistry of ferromanganese nodules from the Gulf of Cadiz: The role of the Mediterranean Outflow Water undercurrent, *J Mar Syst*, 80 (3-4) (2010) 203-218. DOI: 10.1016/j.jmarsys.2009.10.010

17 Muinos S B, Hein J R, Frank M, Monteiro J H, Gaspar L, *et al*., Deep-sea Fe-Mn Crusts from the Northeast Atlantic Ocean: Composition and Resource Considerations, *Marine Georesour Geotechnol*, 31 (1) (2013) 40-70. doi: 10.1080/1064119X.2012.661215

18 Gonzalez F J, Somoza L, Hein J R, Medialdea T, Leon R, *et al*., Phosphorites, Co-rich Mn nodules, and Fe-Mn crusts from Galicia Bank, NE Atlantic: Reflections of Cenozoic tectonics and paleoceanography, *Geochem Geophys Geosystem*, 17 (2) (2016) 346-374, DOI: 10.1002/2015GC005861

19 Hein J R, Konstantinova N, Mikesell M, Mizell K, Fitzsimmons J N, *et al*., Arctic Deep-Water Ferromanganese-Oxide Deposits Reflect the Unique Characteristics of the Arctic Ocean, *Geochem Geophys Geosystem*, 18 (11) (2017) 3771-3800. DOI: 10.1002/2017GC007186

20 Marino E, Gonzalez F J, Lunar R, Reyes J, Medialdea T, *et al*., High-Resolution Analysis of Critical Minerals and Elements in Fe–Mn Crusts from the Canary Island Seamount Province (Atlantic Ocean), *Minerals*, 8 (2018) p. 285. DOI: 10.3390/min8070285

21 Dinesh A C, Nisha, N V, Saju V, Rachna P, Durga P, *et al*., Extensive occurrence of Fe-Mn crusts and nodules on seamounts in the southern Andaman Sea, India, *Curr Sci*, 119 (4) (2020) 704-708. DOI: 10.18520/cs/v119/i4/704-708

22 Jishnu B K, Saju V, Nagasundaram M, Durga P, Madhupriya N, *et al*., Occurrence and distribution of polymetallic nodules and crust in the West Sewell Ridge (WSR), Andaman Sea, Conference paper presented at the *MARICON* (Cochin), 2019, ISBN: 978-81922264-3-9

23 Rajani R P, Manoj R V, Nagasundaram M, Joshi R K & Sethu R J, Hydrothermal manganese mineralization in the Sewell Rise: Evidence for low temperature hydrothermal activity in the Andaman Back Arc Basin, Conference paper presented at the *MARICON* (Cochin), 2019, ISBN: 978-81922264-3-9

24 Saju V, Rajani P R, Rachna P, Sethu R J, Gopakumar B, *et al*., Accumulation and enrichment of platinum group elements in hydrogenous Fe-Mn crust and nodules from the Andaman Sea, India, *Curr Sci*, 120 (1) (2021) 1740-1748.

25 Rajani R P, Manoj R V, Joshi R K, Jishnu B K & Nagasundaram M, Base metals- and Lithium- rich ferromanganese oxide deposits from the South Andaman Sea, Northeastern Indian Ocean: Mode of occurrence and genesis, *J Asian Earth Sci*, 134 (2022) p. 105272. https://doi.org/10.1016/j.jseaes.2022.105272

26 Jiang X D, Sun X M & Guan Y, Biogenic mineralization in the ferromanganese nodules and crusts from the South China Sea, *J Asian Earth Sci*, 171 (2019) 46-59. https://doi.org/10.1016/j.jseaes.2017.07.050